Chapter 6
Numerical Features of CESE Schemes

In this chapter, some remarks are made on the numerical characteristics of the CESE schemes described in foregoing chapters. Due to the special formulation, rigorous analysis of the CESE schemes will take more efforts than that of traditional finite difference schemes. However, it is possible to extend the widely used modified equation analysis, modified wavenumber analysis, and von Neumann stability analysis to the CESE schemes. Here, a stability analysis for the second-order upwind CESE scheme applied to the linear scalar convection equation is presented. Additionally, a rough estimation of the algorithm complexity is presented to show the computational efficiency of the CESE method. In order to demonstrate the accuracy of the CESE method in comparison with established numerical approaches, simulation results of some canonical problems are shown.

6.1 Stability

All CESE schemes in this book are explicit time-stepping schemes. Similar to other explicit schemes, the numerical stability of CESE schemes is closely related to the Courant–Friedrichs–Lewy (CFL) condition. Only when the CFL condition is satisfied, the system can remain numerically stable. Consequently, the time-step size used by a CESE scheme has to be restricted according to the upper bound of the stable CFL number ν for that scheme.

It has been proven in [1, 2] that the stability conditions for the second-order a scheme (Sect. 2.3) and the second-order a–α scheme (Sect. 3.1) are both $\nu \leq 1$. For the second-order upwind CESE scheme (Sect. 3.3), the stable upper bound of the CFL number is also unity. This stability analysis is first given by Jiang et al. [3] and introduced as follows.

For illustrative purpose, we consider the simplest upwind CESE scheme applied to the 1D linear scalar convection equation

C.-Y. Wen et al., *Space–Time Conservation Element and Solution Element Method*,
Engineering Applications of Computational Methods 13,
https://doi.org/10.1007/978-981-99-0876-9_6

$$\frac{\partial u}{\partial t} + a\frac{\partial u}{\partial x} = 0 \tag{6.1}$$

where a is a positive constant. Without using any slope limiter, the upwind CESE scheme for Eq. (6.1) can be written in a matrix form as

$$\boldsymbol{q}_j^n = \boldsymbol{Q}_L \boldsymbol{q}_{j-1/2}^{n-1/2} + \boldsymbol{Q}_R \boldsymbol{q}_{j+1/2}^{n-1/2} \tag{6.2}$$

with the vector of time-marching variables

$$\boldsymbol{q}_j^n = \begin{bmatrix} u_j^n \\ \dfrac{\Delta x}{4}(u_x)_j^n \end{bmatrix}, \tag{6.3}$$

and the coefficient matrices (recall Chap. 3)

$$\boldsymbol{Q}_L = \frac{1}{2}\begin{bmatrix} 1+\nu & 1-\nu^2 \\ -1+\nu & -1+4\nu-\nu^2 \end{bmatrix}, \qquad \boldsymbol{Q}_R = \frac{1}{2}\begin{bmatrix} 1-\nu & -1+\nu^2 \\ 1-\nu & -1+\nu^2 \end{bmatrix}, \tag{6.4}$$

where ν is the CFL number, which is defined as

$$\nu \equiv a\frac{\Delta t}{\Delta x}. \tag{6.5}$$

Following the routine of von Neumann stability analysis, we assume the vector $\boldsymbol{q}$ to be a Fourier component with arbitrary wavenumber k such that

$$\boldsymbol{q}_j^n = \boldsymbol{A}_n(\theta) e^{ij\theta}, \quad (-\pi < \theta \le \pi), \tag{6.6}$$

where $\theta = k\Delta x$ is the reduced wavenumber, and i is the imaginary unit. Substituting Eqs. (6.6) into (6.2) yields

$$\boldsymbol{A}_n(\theta) = \left[\boldsymbol{Q}_L e^{-i\theta/2} + \boldsymbol{Q}_R e^{i\theta/2}\right]\boldsymbol{A}_{n-1/2}(\theta). \tag{6.7}$$

Hence, the amplification matrix for each half step is

$$\begin{aligned} \boldsymbol{M} &= \boldsymbol{Q}_L e^{-i\theta/2} + \boldsymbol{Q}_R e^{i\theta/2} \\ &= \begin{bmatrix} \cos\frac{\theta}{2} - i\nu\sin\frac{\theta}{2} & i(\nu^2-1)\sin\frac{\theta}{2} \\ i(1-\nu)\sin\frac{\theta}{2} & (2\nu-1)\cos\frac{\theta}{2} + i(\nu^2-2\nu)\sin\frac{\theta}{2} \end{bmatrix}. \end{aligned} \tag{6.8}$$

The spectral radius of matrix $\boldsymbol{M}$, denoted as $\rho(\nu, \theta)$, is calculated numerically as a function of the CFL number ($0 \le \nu \le 1$) and reduced wavenumber ($-\pi \le \theta \le \pi$). In Fig. 6.1, it can be seen that $\rho(\nu, \theta) \le 1$ holds for all wavenumbers as long as $0 \le \nu \le 1$. Thus, this second-order upwind CESE scheme is numerically stable when ν

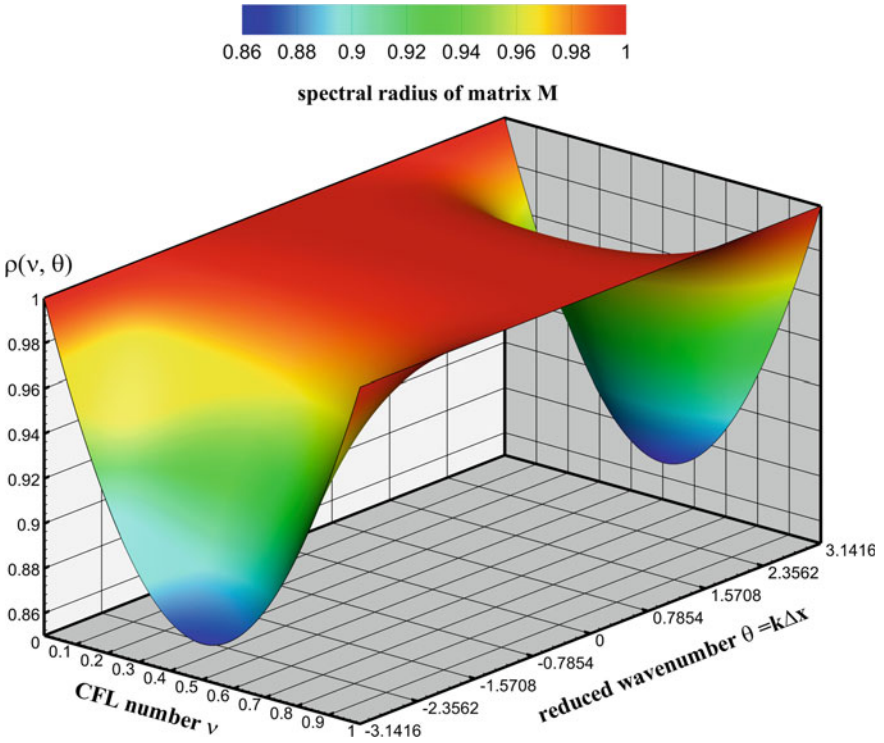

Fig. 6.1 Spectral radius $\rho(\nu, \theta)$ of matrix $\boldsymbol{M}$ in the von Neumann analysis of the upwind CESE scheme. Courtesy of Jiang [3]

is less than or equal to 1. Also shown in Fig. 6.1, as the CFL number approaches 0 or 1, the numerical dissipation in the second-order upwind CESE scheme vanishes.

For high-order CESE schemes, the stability analysis is more complicate and the stable upper bound of the CFL number depends on the scheme's construction. A novel approach to construct highly stable high-order CESE schemes was proposed by Chang [4], using the same space–time stencil as that in the second-order CESE scheme. The same CFL-number constraint for numerical stability (i.e., $\nu \leq 1$) is retained, which is favourable for explicit time-stepping computations.

6.2 Efficiency

The CESE method has a highly compact stencil in space and time, regardless of the order of the scheme. This compactness feature provides the CESE method a great advantage when parallel computation is performed.

For a CESE scheme, the nominal order of accuracy and spatial dimensionality will determine the number of independent variables (denoted by K) to be stored and updated at each solution point. For a M-th-order accurate ($M \geq 2$) and spatially D-dimensional ($D = 1$, 2, or 3) CESE scheme, K can be determined by a precise counting and

$$K(D, M) = \begin{cases} M, & D = 1 \\ M(M+1)/2, & D = 2 \\ M(M+1)(M+2)/6 & D = 3 \end{cases}. \tag{6.9}$$

Notably, the number K in the CESE scheme is the same as the number of degrees of freedom for each cell in the discontinuous Galerkin (DG) scheme. Therefore, if the CESE and DG schemes are of the same order and used to solve the same problem on the same mesh, the memory requirements for a CESE scheme and a DG scheme are comparable.

The CESE method requires neither a reconstruction procedure based on a wide stencil nor a multi-stage time-integration technique. Besides, no upwind operation related to flux calculation is included in central CESE schemes. Nevertheless, the CESE method adopts the Cauchy–Kowalewski procedure to express the temporal derivatives in terms of spatial derivatives. It also takes time to update the spatial derivatives using the algorithms described in Chaps. 3, 4 and 5. The combined effect of all these factors determines the computational speed of the CESE method.

6.3 Accuracy

Generally, the accuracy of a CESE scheme depends on the order of the Taylor expansions, i.e., the degree of the approximation polynomials that are used to approximate unknowns and fluxes within each solution element. To achieve the theoretical M-th order of accuracy of the scheme in space and time, the $(M-1)$-th-order Taylor expansions are needed. According to practical applications, the second-order CESE schemes, including the central and upwind schemes, can usually provide a satisfactory trade-off between accuracy and efficiency.

The ability to capture shock waves and contact discontinuities with high resolution is one of the excellent features of the CESE scheme. Here, two canonical flow problems are used to demonstrate the accuracy of CESE schemes by comparing the numerical simulation results by CESE and other schemes. As the first example, Sod's shock-tube problem [5] is solved by both the CESE method and the finite volume method (FVM). The CESE code is an implementation of the second order a–α scheme described in Chap. 3, while the FVM counterpart incorporates the second-order MUSCL (Monotonic Upstream-centered Scheme for Conservation Laws) reconstruction, the van Leer limiter, and the HLLC Riemann solver. A uniform mesh with 200 cells and a CFL number of 6.9 are employed in both the CESE and the FVM

computations. Density and internal energy distributions from $x = -1$ to $x = 1$ at time $t = 6.5$ computed by CESE and FVM schemes are plotted in Fig. 6.2a and b, respectively, in comparison with the exact solution. As shown in Fig. 6.2, a narrower contact discontinuity is resolved by the CESE scheme than the FVM counterpart. Meanwhile the CESE results match the exact solution better than the FVM results at the tail of the rarefaction wave.

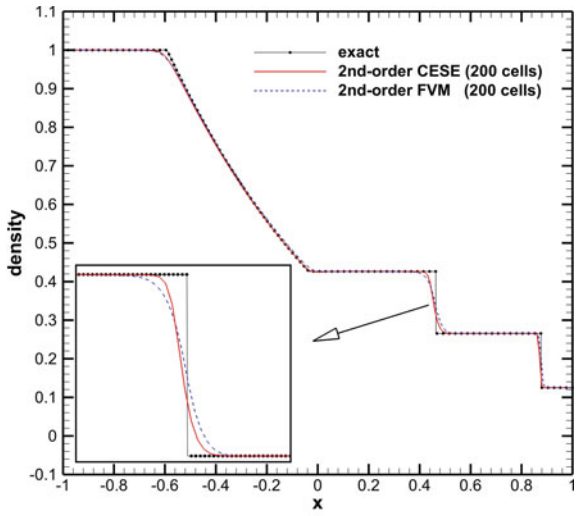

(a) CESE result vs. FVM result: density

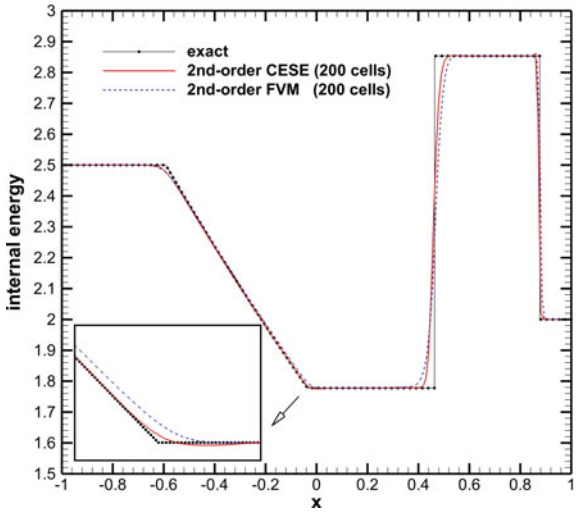

(b) CESE result vs. FVM result: internal energy

Fig. 6.2 Comparison of numerical results of Sod's shock-tube problem by CESE and FVM schemes at dimensionless time $t = 0.5$. Courtesy of Jiang [3]

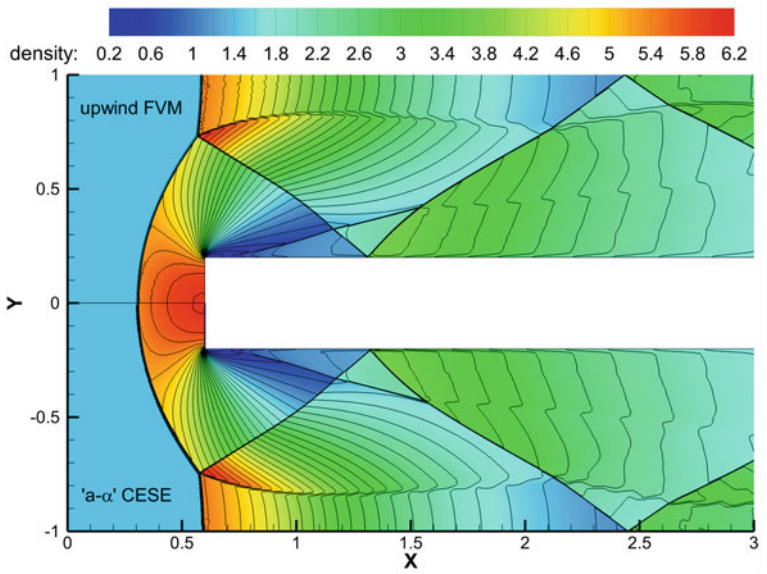

(a) a–α CESE result vs. FVM result

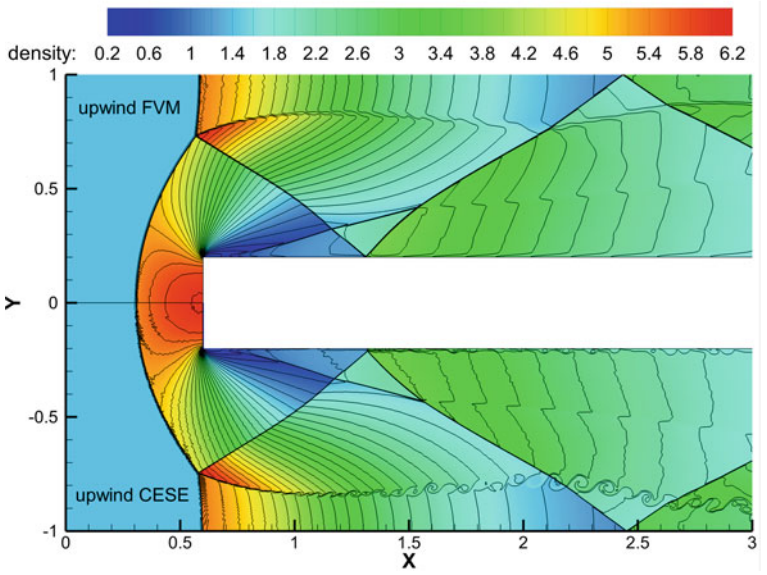

(b) Upwind CESE result vs. FVM result

Fig. 6.3 Comparison of FVM and CESE results for Mach 3 step problem: density contours at time $t = 4.6$. Courtesy of Jiang [3]

In the second example, the problem of a Mach-3 inviscid flow through a 2D tunnel with a forward-facing step inside is solved by three schemes (a–α CESE, upwind CESE, and upwind FVM) of second-order accuracy in space and time. The initial conditions, boundary conditions, and geometrical parameters are the same as that in [6]. The upwind FVM flow solver is provided by Hao et al. [7]. The same computational mesh and the same Courant–Friedrichs–Lewy (CFL) number of 6.95 are employed for all the three schemes. Density fields at time $t = 4.0$ are shown in Fig. 6.3a and b. Compared with the upwind FVM scheme, both the a–α and upwind CESE schemes can accurately capture the structure of shock waves, but only the upwind CESE scheme can resolve the phenomenon of shear-layer instability (see the lower part of Fig. 6.3b), which is not observed in the present a-α CESE and FVM results.

To assess the accuracy of the high-order CESE schemes described in Chap. 5, the Shu–Osher problem and the double Mach-reflection problem were studied intensively in Ref. [8], where the fourth-order CESE scheme provided a good resolution of fine structures in the flows.

References

1. Chang, S. C. (1995). The method of space-time conservation element and solution element—A new approach for solving the Navier-Stokes and Euler equations. *Journal of computational Physics, 119*(2), 295–324.
2. Yang, D., Yu, S., & Zhao, J. (2001). Convergence and error bound analysis for the space-time CESE method. *Numerical Methods for Partial Differential Equations: An International Journal, 17*(1), 64–78.
3. Jiang, Y. Z., Wen, C. Y., & Zhang, D. L. (2020). Space-time conservation element and solution element method and its applications. *AIAA Journal, 58*(12), 5408–5436.
4. Chang, S.C. (2010). A new approach for constructing highly stable high order CESE schemes. In *48th AIAA Aerospace Sciences Meeting Including the New Horizons Forum and Aerospace Exposition.*
5. Sod, G. A. (1978). A survey of several finite difference methods for systems of nonlinear hyperbolic conservation laws. *Journal of computational physics, 27*(1), 1–31.
6. Woodward, P., & Colella, P. (1984). The numerical simulation of two-dimensional fluid flow with strong shocks. *Journal of computational physics, 54*(1), 115–173.
7. Hao, J., Wang, J., & Lee, C. (2017). Numerical simulation of high-enthalpy double-cone flows. *AIAA Journal, 55*(7), 2471–2475.
8. Shen, H., Wen, C. Y., Liu, K. X., & Zhang, D. L. (2015). Robust high-order space–time conservative schemes for solving conservation laws on hybrid meshes. *Journal of Computational Physics, 281*, 375–402.